

**Title (15 Words max):**

# Identifying and Managing Reversible Capacity Losses that Falsify Cycle Ageing Tests of Lithium-ion Cells

Author Names: Robert Burrell<sup>1</sup>, Alana Zulke<sup>1</sup>, Peter Keil<sup>2</sup>, Harry Hoster<sup>1</sup>

Affiliation(s): <sup>1</sup>*Department of Chemistry, Lancaster University, Lancaster, LA1 4YB, United Kingdom*

<sup>2</sup>*Battery Dynamics GmbH, Lichtenberg Strasse 85748, München, Germany*

<sup>z</sup>Corresponding Author E-mail Address [a.zulke@lancaster.ac.uk]

## **Abstract**

We report on a cycle ageing study of commercial NCA/Gr+Si cells, in which reversible capacity fluctuations turn a central experimental finding upside down: an upper voltage limit of 4.1 V seems to cause faster degradation than going all the way to 4.2 V. The underlying effect is the reversible loss of lithium inventory into passive anode overhang areas. We demonstrate how the resulting artefact arises from a combination of slow transport processes and the related time periods spent in specific state-of-charge regions. We propose an alternative visualisation tool to identify and manage such artefacts, often neglected in typical ageing studies.

## **Introduction**

Cycle ageing studies are essential tools to predict the technically important cycle-life of lithium-ion battery (LIB) cells and to quantify irreversible capacity losses.<sup>1-3</sup> They involve repeated charge-discharge cycles with fixed protocols but for varied parameters such as depth-of-discharge, C-rate, or voltage window. Because those studies are inherently slow and expensive, results may often have to be derived from a few hundred cycles which are conducted as fast as possible, i.e., minimising resting periods to the technically necessary minimum. It is in principle known that experimentally derived degradation rates can be “poisoned” by

reversible capacity fluctuations caused, e.g., by (reversible) loss of lithium into the passive anode overhang areas<sup>4-7</sup> or inhomogeneities of lithium distribution within the active material<sup>8-12</sup>, including the formation of a dense covering layer on the surface of the anode<sup>7,13,14</sup>. Possible effects of gradients of pressure<sup>15</sup> or temperature<sup>16</sup> were also discussed.

In this communication, we will demonstrate that reversible losses can falsify cycle ageing studies more severely than just adding evenly spread biases. “Evenly spread” refers to a situation where a modified experimental variable would not trigger larger or smaller contributions from the reversible processes to the experimentally determined capacity fade. The biggest weakness of cycle ageing studies is that they don’t explicitly account for the time periods spent in certain voltage and state-of-charge (SoC) regions, even though the experimental protocols allow those periods to vary. As an example, we will demonstrate how sluggish transport processes in certain SoC-regions can extend constant voltage phases in standard charging protocols. This enhances the contribution of reversible side reactions to an extent that it inverts the outcome of the degradation tests if compared to the actual trend in irreversible degradation. We will show how this influence can be compensated by a minor (yet time consuming) modification of the experiment, and how timesheet-map visualisations of the experimental data sets can help to flag the expected level of data contamination by such artefacts.

## **Experimental**

High-energy 18650 Samsung cells with a rated capacity of 3.35 Ah at 1.7 A and 25°C were used in these experiments. These cells are comprised of graphite-silicon (Gr-Si) as the anode material and Nickel-Cobalt-Aluminium (NCA) oxide as the cathode material (cf. table 1). For cycling we used BaSyTec CTS battery cyclers and Memmert IP260 PP thermal chambers at 25°C. All cells were charged using 1.0 A (0.29 C) and 1.7 A (0.5 C) in alternating blocks of 48 cycles each (i.e. 48 cycles @ 0.29 C followed by 48 cycles @ 0.5 C). The blocks of 48 cycles were chosen as part of another experimental investigation in which we explored the impact of different charging alternations. However, those effects will not be discussed here. All cells were discharged at 1.0 A. We used six different voltage windows by combining two and three cut-off voltages for charge and discharge, respectively (cf. table 2). One cell was used for each test

condition, however the cells show excellent reproducibility both in an initial batch performance test (see figure s1) and under load (see figure s2). Charging and discharging was conducted at constant current (CC) and constant current constant voltage (CCCV, CV phase current cut-off of  $0.1 \text{ A} = 0.029 \text{ C}$ ) modes, respectively.

Galvanostatic intermittent titration technique (GITT) was carried out on a Biologic BCS 815 system, using 10 min pulses of 1.25 mA with subsequent 30 min of relaxation throughout a complete charge from 2.5 V to 4.2 V. Effective diffusion coefficients were calculated using Sand's approach<sup>17</sup>.

Every 48 cycles, all cells underwent performance “check-up” tests at 25°C within the full-cell voltage limits 2.5 V ... 4.2 V: 1.0 A CC discharge to determine capacity; 0.25 A charge for differential voltage analysis (DVA); and a final set of 3.0 A discharge pulses at 50% SoC for the estimation of DC resistances.

To test the CCCV charging times from 2.5 V to 4.1 V and 4.2 V, charging tests were performed with four charging currents on a fresh cell. Starting from the lowest current, five charge/discharge procedures were performed at each charging current: 0.5 A, 1.0 A, 1.5 A and 2.0 A. 1.0 A CC discharges were used throughout. After every five charge/discharge sequences, the cells were rested for 5 hours to allow sufficient relaxation. The values presented in figure 1b are an average of all five times obtained at each charging current.

## Results and Discussion

All cells show a near linear capacity fade through to 528 cycles, although with different slopes (see Figure 1a). Greater losses are seen for cells cycled to lower cut-off voltages, with 2.5 V standing out in particular. That is to be expected and was previously attributed to a combination of higher intercalation-related stresses experienced by the (almost) completely delithiated graphite and the likely effects of volume fluctuations from silicon.<sup>18,19</sup> Increasing the charge voltage window, on the other hand, produces a different trend: raising the charge cut-off from 4.1 to 4.2 V *reduces* the capacity fade by 1% over the 528 cycles. This trend is seen for all cells, regardless of their discharge cut-off voltage. The value of 1% variation is significant, given a cell-to-cell variation of around 0.3% (11 mAh) in initial batch screening tests (beginning of life, at C/3, see figure s1) and a difference of ~0.2% for reference tests under

identical load conditions over ~350 cycles (see figure s2). The gap in relative capacity between cells charged to 4.1 V vs. 4.2 V seems to be created during the early cycles and is then largely maintained for the rest of the data points (Figure 1a). Hence, the associated capacity loss must be technically capped.

Charging to 4.1 V takes longer than to 4.2 V in CCCV mode. This is illustrated in Figure 1b, which displays the durations of CCCV charges to both voltages, starting at 2.5 V and at 4 different charging currents. For each current value, the plotted duration reflects an average over 5 consecutive cycles of a fresh cell. The experiments went from the lowest to the highest charging currents with significant rest periods in between. Relative contributions from constant current (CC) and constant voltage (CV) phases to the total CCCV charging time are distinguished by colour. As expected, a CC charge to 4.1 V takes less time than a CC charge to 4.2 V. However, the current relaxation during the CV phase takes much longer at 4.1 V. For example, the CV phase accounts for over half the total charging time for a 2.0 A charge. Although the proportion of time spent in the CV phase to CC phase reduces as the charging current is reduced, the length of the CV phase does not significantly reduce with charging current.

The longer CV phase at 4.1 V results from slower Li ion transport in the anode as compared to 4.2 V, which hinders the relaxation processes during the CV phase. This picture is confirmed by GITT measurements of an anode half-cell (information on the coin cell manufacture can be found in the supplementary information). Figure 1c shows the effective diffusion coefficients as a function of the degree of lithiation, which produces a profile very close to findings for other cells<sup>20</sup> (note that the absolute values might differ for reasons related to the models underpinning the GITT data interpretation and technical features of the specific laboratory cell). We rationalize the longer CV phase at 4.1 V based on the highlighted aspects in figures 1c and d, which show the effective diffusion coefficient of  $\text{Li}^+$  in the anode and the anode equilibrium voltage curve during lithiation, respectively. By identifying the location of the central graphite peak (at  $\text{Li}_{0.5}\text{C}_6$ ) in the DVA curve of a fresh cell, the anode was calculated to be ~14% oversized by mass loading. Therefore, at 4.1 V and 4.2 V, the anode is approximately 75% and 87% lithiated, respectively, which allows identifying those very regions in figure 1c. The effective diffusion coefficient in the anode is up to an order of magnitude lower when the full

cell is at 4.1 V as compared to 4.2 V. This retards the approach of the user-defined cut-off current that terminates the CV phase. In the same full-cell voltage region, the effective diffusion coefficients in the cathode are much higher (see figure s3). This confirms the idea that sluggish anode processes are rate determining. We can also verify the reduced mobility of  $\text{Li}^+$  within the graphite from the perspective of the phase transitions reflected in the anode equilibrium voltage curve, as seen in figure 1d. It has been hypothesised that “flat” regions of voltage-capacity profiles provide an insufficient driving force to re-homogenise the lithium distribution across the electrode in the event that it has become non-uniform.<sup>21,22</sup> This is because a given concentration gradient would result in smaller spatial variations of the chemical potential, the driving force behind diffusion. In the case of the data presented here, it becomes clear that when the full cell potential is at 4.1 V, the local anode potential is located towards the end of a plateau (co-existence of a two-phase equilibria region<sup>23</sup>) whereas when at 4.2 V, the local anode potential is in a steeper region. We stress that the variation of only 100 mV in the full cell cut-off voltage in this region can translate into significantly different thermodynamic states in the anode material, thus drastically altering the driving force for  $\text{Li}^+$  mobility.

To capture time-domain effects in cell cycling experiments, we propose introducing 2D histogram timesheets (resembling heatmaps) as the ones in Figure 2a and b. These summarise all 528 cycles of 2 cells with the same discharging cut-off voltage, but different charging cut-off voltages and were produced by a code that analysed the raw data of battery test channels in terms of how much time was spent in which regime in a current/voltage map. Apart from providing a quick high-level visual diary, they also give an idea about the relaxation current profiles in the CV phases at 4.1 vs. 4.2 V: after reaching the respective voltages, the time spent in the CV phase is largely similar for both cut-off voltages until around 0.55 A. According to Figure 2c, the 4.1 V cell then spends up to an order of magnitude more time at low relaxation currents than the one at 4.2 V. This disproportionate increase in charging time could largely be avoided by raising the user-determined cut-off current value in the protocol design, which would avoid these time-costly periods and avoid the artefacts that come with them.

Because cells charged to 4.1V spend increased lengths of time at high SoC than those charged to 4.2 V, the cyclable lithium content will thus be influenced by the anode overhang areas, which correspond to the perimeter portions of the anode active material that do not have

a direct cathode counterpart (see Figure 4).<sup>24</sup> They act as a lithium sink or a lithium source, depending on the voltage / SoC at which the cell is held.<sup>25</sup> Li flow between active and passive anode areas (sometimes referred to as “passive electrode” effect) is slow and equilibration occurs on the time scale of weeks (see Figure 3). The anode overhang of cells stored at lower SoC will have a similarly small Li content as the active part of the anode. Subsequent operation of such cells at higher time-averaged SoC will induce a slow but steady net lithium flow from the now (on average) more lithiated active anode into the anode overhang. In this picture, the longer time spent in the CV phase at 4.1 V vs. 4.2 V causes more loss of lithium inventory into the anode overhang, and thus the additional capacity loss observed in the cycle ageing experiments (Figure 1a).

To disentangle the reversible capacity losses (flow into overhang) from the irreversible ones (actual degradation) one has to recover lithium inventory from the overhang areas. This is achieved by storing all cells at lower SoC at the end of the cycle ageing experiment. Figure 3 shows the relative capacity changes when the cells are stored for 12 weeks at 50% SoC, followed by an additional 12 weeks at 0% SoC. These calendar storage periods were performed immediately after the cycling periods, therefore, at  $t=0$ , the relative capacities displayed in figure 3 are the same relative capacities after 528 cycles (last datapoints in figure 1a). During the first 12 weeks of storage at 50% SoC, all cells but one showed a slight recovery in capacity. Interestingly, the cells that were previously cycled to 4.1 V recovered the most capacity to reach a point similar to their 4.2 V counterparts, with maximum recovery of 1%. When dropped to 0% SoC, all cells showed a significant recovery in capacity, particularly apparent again for the cells previously cycled to 4.1 V, which showed a maximum recovery of 3.5%.

Hence, the irreversible capacity loss during cycle ageing was indeed bigger for the cells charged to 4.2 V as compared to 4.1 V. The most straightforward way of measuring this is to store the cells at 0% SoC, interrupted only by a few check-up cycles. This is in line with the previously proposed practise of introducing rest period between blocks of continuous cycling.<sup>6,10,22</sup>

## Summary

Laboratory-based lithium ion cell degradation studies must disentangle reversible and

irreversible capacity changes to achieve meaningful results. Our brief study on the impact of voltage window variations on diagnosed cell degradation revealed four main findings:

- (1) The time spent in the constant-voltage phase at the end of charge in a typical cycle ageing study depends on Li transport at the respective SoC in the given anode material. Longer waiting periods mean more influence of slow side reactions, including but not restricted to the reversible loss of Lithium into overhang areas.
- (2) For instance, upper voltage limits of 4.1 V and 4.2 V lead to average constant-voltage periods of 1.6 and 0.6 hours, respectively, if the same current threshold is applied. This increased spill-over of Lithium from the active into the passive (“overhang”) anode region, making the capacity losses look larger for 4.1 V.
- (3) Rest periods at low SoC bring back most of the Lithium from overhang regions, thus allowing again for quantitative comparison within the set of samples. In the specific case, this inverts our findings: 4.2 V as upper voltage limit does actually lead to faster cycle ageing than 4.1 V, as one would expect for a larger voltage window.
- (4) To identify potential sources of artefacts, the time periods spent in certain voltage and current regimes should be routinely considered in studies that focus on cycles or charge throughput rather than time. We presented a 2D time-sheet histogram that serves this purpose. This tool also flags potential cost-saving opportunities, e.g., via adjusting cut-off current levels to shorten artificially long CV phases.

The relative impact of reversible losses on the diagnosed irreversible ones is high because modern lithium ion cells degrade very slowly. The technological importance of an accurate understanding and capturing of cell degradation demands concerted efforts to develop informed and transparent experimental standards.

## References

1. M. Ecker, N. Nieto, S. Käbitz, J. Schmalstieg, H. Blanke, A. Warnecke, and D. U. Sauer, *J. Power Sources*, **248**, 839–851 (2014).

2. F. Benavente-Araoz, M. Varini, A. Lundblad, S. Cabrera, and G. Lindbergh, *J. Electrochem. Soc.*, **167**, 040529 (2020).
3. S. Gantenbein, M. Schönleber, M. Weiss, and E. Ivers-Tiffée, *Sustain.*, **11**, 1–15 (2019).
4. B. Gyenes, D. A. Stevens, V. L. Chevrier, and J. R. Dahn, *J. Electrochem. Soc.*, **162**, A278–A283 (2014).
5. M. Lewerenz, thesis, RWTH Aachen University (2018).
6. M. Lewerenz, P. Dechent, and D. U. Sauer, *J. Energy Storage*, **21**, 680–690 (2019).
7. M. Lewerenz, A. Warnecke, and D. U. Sauer, *J. Power Sources*, **354**, 157–166 (2017).
8. M. Lewerenz and D. U. Sauer, *J. Energy Storage*, **18**, 421–434 (2018).
9. M. Lewerenz, A. Marongiu, A. Warnecke, and D. U. Sauer, *J. Power Sources*, **368**, 57–67 (2017).
10. B. Epding, B. Rumberg, H. Jahnke, I. Stradtman, and A. Kwade, *J. Energy Storage*, **22**, 249–256 (2019).
11. F. Grimsmann, T. Gerbert, F. Brauchle, A. Gruhle, J. Parisi, and M. Knipper, *J. Energy Storage*, **15**, 17–22 (2018).
12. J. P. Fath, D. Dragicevic, L. Bittel, A. Nuhic, J. Sieg, S. Hahn, L. Alsheimer, B. Spier, and T. Wetzel, *J. Energy Storage*, **25**, 100813 (2019).
13. M. Lewerenz, A. Warnecke, and D. U. Sauer, *J. Power Sources*, **369**, 122–132 (2017).
14. M. Klett, J. A. Gilbert, K. Z. Pupek, S. E. Trask, and D. P. Abraham, *J. Electrochem. Soc.*, **164**, A6095–A6102 (2017).
15. T. C. Bach, S. F. Schuster, E. Fleder, J. Müller, M. J. Brand, H. Lormann, A. Jossen, and G. Sextl, *J. Energy Storage*, **5**, 212–223 (2016).
16. M. Klett, R. Eriksson, J. Groot, P. Svens, K. Ciosek Högström, R. W. Lindström, H. Berg, T. Gustafson, G. Lindbergh, and K. Edström, *J. Power Sources*, **257**, 126–137 (2014).
17. P. Bai, J. Li, F. R. Brushett, and M. Z. Bazant, *Energy Environ. Sci.*, **9**, 3221–3229 (2016).
18. V. A. Sethuraman, L. J. Hardwick, V. Srinivasan, and R. Kostecki, *J. Power Sources*, **195**, 3655–3660 (2010).
19. M. Wetjen, D. Pritzl, R. Jung, S. Solchenbach, R. Ghadimi, and H. A. Gasteiger, *J. Electrochem. Soc.*, **164**, A2840–A2852 (2017).
20. M. Ecker, T. K. D. Tran, P. Dechent, S. Käbitz, A. Warnecke, and D. U. Sauer, *J. Electrochem. Soc.*, **162**, A1836–A1848 (2015).
21. M. Naumann, F. Spingler, and A. Jossen, *J. Power Sources*, **451**, 227666 (2020).
22. F. B. Spingler, M. Naumann, and A. Jossen, *J. Electrochem. Soc.*, **167**, 040526 (2020).
23. M. P. Mercer, M. Otero, M. Ferrer-Huerta, A. Sigal, D. E. Barraco, H. E. Hoster, and E. P. M. Leiva, *Electrochim. Acta*, **324**, 134774 (2019).
24. J. Wilhelm, S. Seidlmayer, P. Keil, J. Schuster, A. Kriele, R. Gilles, and A. Jossen, *J. Power Sources*, **365**, 327–338 (2017).
25. M. Lewerenz, J. Münnix, J. Schmalstieg, S. Käbitz, M. Knips, and D. U. Sauer, *J. Power Sources*, **345**, 254–263 (2017).

---

**Table I. Cell Information for Samsung 35E3**

Cell Type	18650		
Cell Chemistry	Nickel	Cobalt	Aluminium/Silicon-Graphite
Max cont. charge/discharge current	2.0 A/8.0 A		
Upper and lower cut-off voltage	4.2 V/2.5 V		

---

---

**Table II. Further details for charge/discharge cut-off voltages, SoC ranges and mean SoCs**

Charge cut-off voltage/V	Discharge cut-off voltage/V	SoC Range	Mean SoC (fresh cell)
4.2	3.4	8.7 – 100%	54%
4.2	3.1	1.5 – 100%	51%
4.2	2.5	0 – 100%	50%
4.1	3.4	8.7 – 86.5%	48%
4.1	3.1	1.5 – 86.5%	44%
4.1	2.5	0 – 86.5%	43%

---

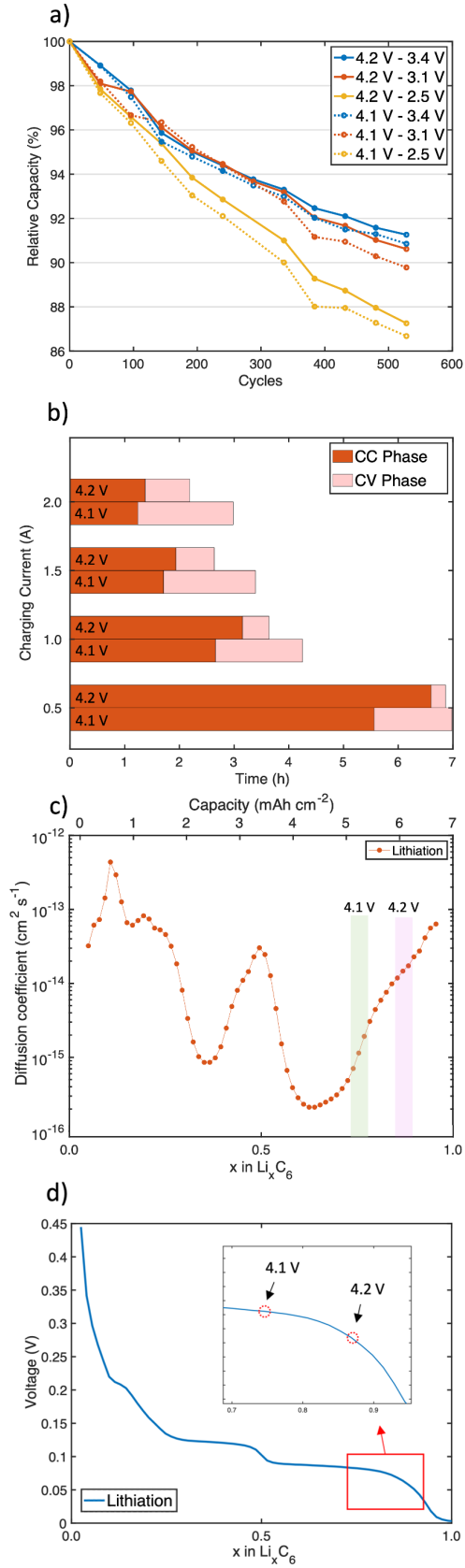


**Figure 1.** (a) Relative capacity vs cycle number for all 6 cycling voltage windows, (b) CCCV charging time showing the length of both CC and CV portions at four different charging currents, (c) GITT-based effective diffusion coefficients vs. degree of lithiation ( $x$ ) in an anode half-cell during charge, (d) equilibrium voltage

vs degree of lithiation of the anode during lithiation.

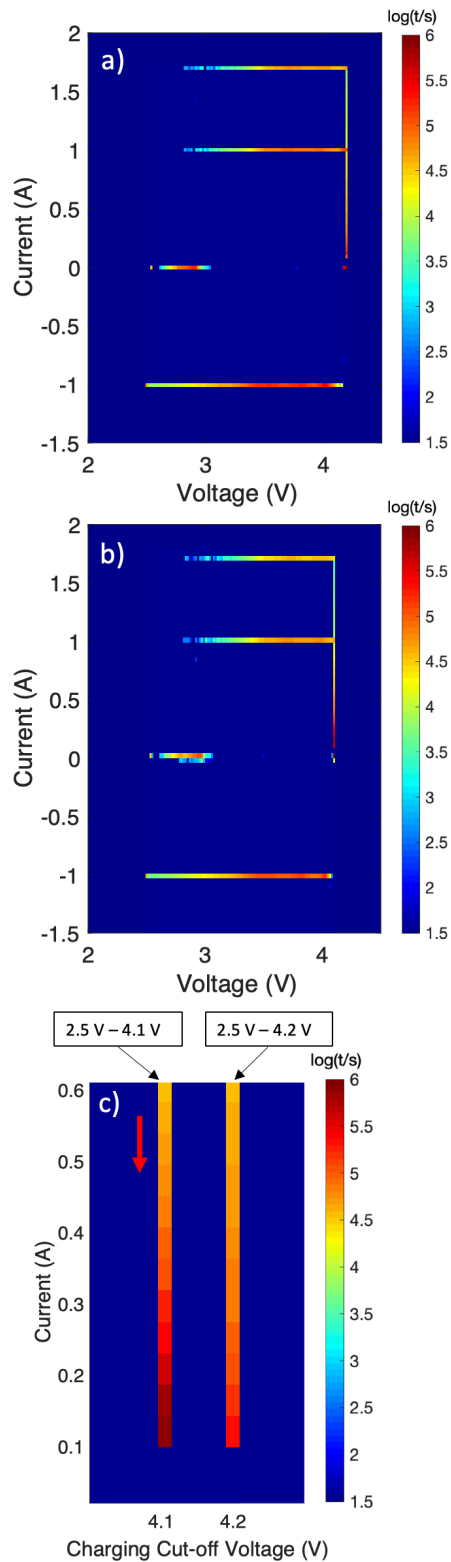


**Figure 2.** 2D time-sheet histogram showing the time spent in different current vs. voltage regions during the cycle degradation experiments over 528 cycles (cf. figure 1a). (a) entire dataset for the cell cycle window 4.2 V and 2.5 V; (b) entire dataset for the cell cycle window 4.1 V and 2.5 V (b) zoom into the CV phases for both cells with the cycling windows 2.5 V - 4.1 V and 2.5 V - 4.2 V. The red arrow denotes the direction of the current change during the CV phase.

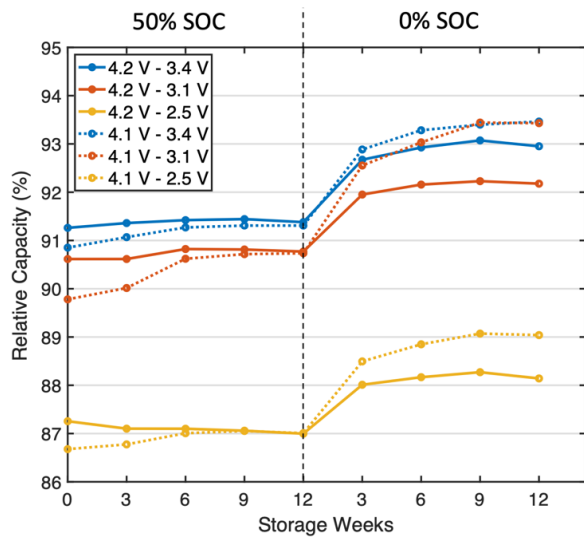


**Figure 3.** Relative capacity vs storage weeks during calendar storage at 50% and 0% SoC ( $T = 25\text{ }^{\circ}\text{C}$ ). This figure is a continuation of the relative capacity curves in figure 1a.

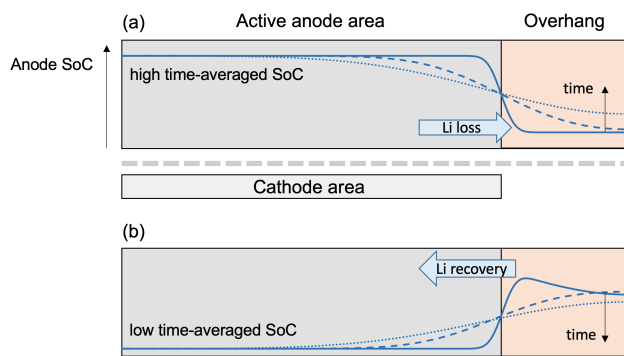


**Figure 4.** Li exchange with overhang for the extreme cases of (a) high and (b) low time-averaged SoC. Solid line: Li concentration after reaching a new average state-of-charge; Li concentration gradients drive Li diffusion; dashed lines: Li concentration change after some weeks.